Cosmological test of local position invariance from the asymmetric galaxy clustering

Shohei Saga, Atsushi Taruya, Michel-Andrès Breton, Yann Rasera

Monthly Notices of the ROYAL ASTRONOMICAL SOCIETY

MNRAS **524,** 4472–4481 (2023) https://doi.org/10.1093/mnras/stad2191
Advance Access publication 2023 July 21

Cosmological test of local position invariance from the asymmetric galaxy clustering

Shohei Saga [1,2]★ Atsushi Taruya [3,4] Yann Rasera[5] and Michel-Andrès Breton[6,7,8]

[1]*Institut d'Astrophysique de Paris, Sorbonne Universtié, CNRS, UMR7095, 98bis boulevard Arago, F-75014 Paris, France*
[2]*Laboratoire Univers et Théories, Observatoire de Paris, Université PSL, Université de Paris, CNRS, F-92190 Meudon, France*
[3]*Center for Gravitational Physics, Yukawa Institute for Theoretical Physics, Kyoto University, Kyoto 606-8502, Japan*
[4]*Kavli Institute for the Physics and Mathematics of the Universe (WPI), The University of Tokyo Institutes for Advanced Study, The University of Tokyo, 5-1-5 Kashiwanoha, Kashiwa, Chiba 277-8583, Japan*
[5]*Laboratoire Univers et Théories, Université de Paris, Observatoire de Paris, Université PSL, CNRS, F-92190 Meudon, France*
[6]*Aix Marseille Univ, CNRS, CNES, LAM, Marseille 13013, France*
[7]*Institute of Space Sciences (ICE, CSIC), Campus UAB, Carrer de Can Magrans, s/n, E-08193 Barcelona, Spain*
[8]*Institut d'Estudis Espacials de Catalunya (IEEC), Carrer Gran Capità 2-4, E-08193 Barcelona, Spain*

Accepted 2023 July 14. Received 2023 June 10; in original form 2023 January 21

ABSTRACT

The local position invariance (LPI) is one of the three major pillars of Einstein equivalence principle, ensuring the space–time independence on the outcomes of local experiments. The LPI has been tested by measuring the gravitational redshift effect in various depths of gravitational potentials. We propose a new cosmological test of the LPI by observing the asymmetry in the cross-correlation function between different types of galaxies, which predominantly arises from the gravitational redshift effect induced by the gravitational potential of haloes at which the galaxies reside. We show that the ongoing/upcoming galaxy surveys give a fruitful constraint on the LPI-violating parameter, α, in the distant universe (redshift $z \sim 0.1$–1.8) over the cosmological scales (separation $s \sim 5$–$10\,h^{-1}$ Mpc) that have not yet been explored, finding that the expected upper limit on α can reach 0.03.

Key words: (*cosmology*:) dark matter – (*cosmology*:) large-scale structure of Universe.

1 INTRODUCTION

Since its foundation, general relativity has been the essential framework to describe gravity in astronomy and cosmology. An important building block of general relativity is the Einstein equivalence principle. As part of it, the local position invariance (LPI) has been playing a special role even for alternative theories of gravity. It states that the outcome of any local non-gravitational experiment is independent of where and when it is performed. An important consequence of the LPI is predicting the gravitational redshift effect. It indicates that the gravitational redshift, $z_{\rm grav}$, between two identical clocks located at different gravitational potentials, $\Delta\phi$, can be given by $z_{\rm grav} = \Delta\phi$ (the speed of light is taken as unity). If the LPI is violated, this relation has to be modified, and it is commonly parametrized in the form (e.g. Will 2018):

$$z_{\rm grav} = (1+\alpha)\Delta\phi, \tag{1}$$

where the non-zero value of α implies the LPI violation.

Pound & Rebka (1959) and Pound & Snider (1965) have made the first successful high-precision measurements of the gravitational redshift effect due to the gravitational potential of the Earth (the Pound–Rebka–Snider experiment), constraining the LPI-violating parameter with an accuracy of $\alpha \lesssim O(10^{-2})$. After these pioneering works, the constraint on α has been obtained and improved by many measurements, for instance, spacecraft measurements (Vessot et al. 1980; Krisher, Anderson & Campbell 1990), solar-spectra measurements (Lopresto, Schrader & Pierce 1991; González Hernández et al. 2020), and null experiments, which constrain the difference in α between different kinds of atomic clocks in the laboratory (Leefer et al. 2013; Peil et al. 2013). Recent null experiment puts the upper bound on the LPI-violating parameter by $\alpha < O(10^{-6})$ (Peil et al. 2013). The limits on α obtained above cover a range of $10^{-15} \lesssim \Delta\phi \lesssim 10^{-6}$. Interestingly, Amorim et al. (2019) and Mediavilla & Jiménez-Vicente (2021) have recently measured the stellar/quasar spectrum near the galactic centre supermassive black hole and gave a limit on an LPI violation of $\alpha \lesssim 10^{-2}$ with a potential difference $10^{-4} \lesssim \Delta\phi \lesssim 10^{-2}$.

In this paper, we propose a novel cosmological test of the LPI, probing a new region $10^{-6} \lesssim \Delta\phi \lesssim 10^{-4}$, by using the measurements of galaxy redshift surveys (this range is also covered by the surface gravity of stars, but separating the surface gravity from the systematic effects is still difficult e.g. Dai, Li & Stojkovic 2019; Moschella et al. 2022). The observed galaxy distributions via spectroscopic measurement are apparently distorted due to the special and general relativistic effects (e.g. Sasaki 1987; Matsubara 2000; McDonald 2009; Croft 2013; Bonvin, Hui & Gaztañaga 2014; Yoo 2014; Tansella et al. 2018). Some of the relativistic effects induce asymmetric distortions along the line of sight when cross-correlating different types of galaxies, leading to a non-vanishing dipole.

Bonvin & Fleury (2018) and Bonvin, Oliveira Franco & Fleury (2020) have pointed out that the large-scale dipole signal can test

★ E-mail: saga@iap.fr

the weak equivalence principle. In contrast, based on the numerical simulations and analytical model, we have recently shown that the small-scale dipole is dominated by the gravitational redshift effect mainly arising from the gravitational potential of dark matter haloes (Breton et al. 2019; Saga et al. 2020). Further, we found that such a signal can be detected from upcoming galaxy surveys at a statistically significant level (Saga et al. 2022; see Beutler & Di Dio 2020, for a similar forecast based on a different approach). Note that even the current data set of galaxy clustering and clusters of galaxies provide a marginal detection (Wojtak, Hansen & Hjorth 2011; Kaiser 2013; Jimeno et al. 2015; Sadeh, Feng & Lahav 2015; Alam et al. 2017; Cai et al. 2017; Mpetha et al. 2021). We thus anticipate that the detected dipole signals from future surveys enable us to measure the gravitational redshift effect, offering the LPI test at cosmological scales.

Motivated by these, we present a quantitative analysis for the forecast constraint on the LPI-violating parameter α. In doing so, we use an analytical model that reproduces numerical simulations quite well (Saga et al. 2020, 2022). Taking two major systematics arising from off-centred galaxies into account, we demonstrate that future galaxy surveys will offer an insightful cosmological test of the LPI, uncovering the parameter space that has not been explored so far.

This paper is organized as follows: In Section 2, we present the model of the dipole moment based on our previous works (Saga et al. 2020, 2022), in which the major relativistic effects, the gravitational redshift, and transverse Doppler effects are taken into account. In Section 3, we derive the expected constraint on the LPI-violating parameter α by ongoing and upcoming galaxy redshift surveys. Section 4 is devoted to summary and discussions. Appendices A, B, and C provide, respectively, the derivation of the analytical model for the dipole, the model of the non-perturbative terms involved in the dipole, and the details of the Fisher analysis for deriving uncertainty in the bias parameters, which is used in obtaining the constraint on α.

2 RELATIVISTIC DIPOLE

Let us recall that the observed galaxy position via spectroscopic surveys receives relativistic corrections through the light propagation in an inhomogeneous universe on top of the cosmic expansion. Consequently, the observed source position, $\boldsymbol{s}$, differs generally from the true position, $\boldsymbol{x}$. Taking the major effects into account, their relation becomes

$$\boldsymbol{s} = \boldsymbol{x} + \frac{1}{aH}\left[(\boldsymbol{v}\cdot\hat{\boldsymbol{x}}) - \phi_{\rm halo} + \gamma v_{\rm g}^2\right]\hat{\boldsymbol{x}}, \tag{2}$$

with $\hat{\boldsymbol{x}}$ being the unit vector, $\hat{\boldsymbol{x}} = \boldsymbol{x}/|\boldsymbol{x}|$. The quantities a, H, and $\boldsymbol{v}$ are a scale factor, Hubble parameter, and peculiar velocity of galaxies, respectively. The explicit form of other minor contributions are found in e.g. Yoo (2010), Bonvin & Durrer (2011), and Challinor & Lewis (2011). In equation (2), three contributions in the square bracket are, from the first to third terms, (i) the longitudinal Doppler effect induced by the galaxy peculiar motion, (ii) gravitational redshift effect arising from the potential of the halo at the galaxy position, $\phi_{\rm halo}$[1], and finally, (iii) sum of transverse Doppler, light-cone, and surface brightness modulation effects mainly due to the virialized random motion of galaxies, $v_{\rm g}^2$ (Kaiser 2013; Jimeno et al. 2015; Cai et al. 2017; Mpetha et al. 2021). We introduced a parameter γ and use $\gamma = -5/2$ as a fiducial value, taken from Kaiser (2013). We will discuss the impact of the uncertainty in this parameter later. Since the second and third terms largely depend on the halo properties of targeted galaxies, they are systematically treated as a deterministic constant rather than a stochastic variable, determined solely by the halo masses. In equation (2), relativistic corrections systematically change the observed position along the specific direction $\hat{\boldsymbol{x}}$. This apparently produces an asymmetry in the galaxy clustering, and taking a pair of galaxies with different sizes of relativistic corrections results in a non-vanishing dipole (see equation 3).

With the mapping relation in equation (2) and the number conservation, the observed number density fluctuation of the galaxy population X, $\delta_{\rm X}^{\rm (S)}(\boldsymbol{s})$ is related to the real-space galaxy density field, $\delta_{\rm X}(\boldsymbol{x})$. Furthermore, the galaxy distribution is a biased tracer of matter fluctuations. Our assumption here is that it is simply related to the linear matter fluctuations $\delta_L(\boldsymbol{x})$ through $\delta_{\rm X}(\boldsymbol{x}) = b_{\rm X}\delta_L(\boldsymbol{x})$, with the linear bias parameter $b_{\rm X}$ to be determined observationally. Treating the density fluctuations and relativistic corrections perturbatively, the quantity $\delta_{\rm X}^{\rm (S)}$ is solely expressed in terms of δ_L (Saga et al. 2022).

We then compute the correlation function between the galaxy populations X at $\boldsymbol{s}_1$ and Y at $\boldsymbol{s}_2$, $\xi(\boldsymbol{s}_1,\boldsymbol{s}_2) \equiv \left\langle \delta_{\rm X}^{\rm (S)}(\boldsymbol{s}_1)\delta_{\rm Y}^{\rm (S)}(\boldsymbol{s}_2)\right\rangle$ with $\langle\cdots\rangle$ being the ensemble average. Without loss of generality, we write it as a function of the separation $s = |\boldsymbol{s}_2 - \boldsymbol{s}_1|$, line-of-sight distance $d = |(\boldsymbol{s}_1 + \boldsymbol{s}_2)/2|$, and directional cosine between the line of sight and separation vectors, $\mu = \hat{\boldsymbol{s}}\cdot\hat{\boldsymbol{d}}$. The dipole moment of the correlation function characterizing the asymmetric galaxy clustering is defined by $\xi_1(s,d) = \frac{3}{2}\int_{-1}^{1}{\rm d}\mu\,\mu\,\xi(s,d,\mu)$. For the scales of $s/(h^{-1}\,{\rm Mpc}) \lesssim 30$ in the distant universe, the terms of order $O((s/d)^2)$ are small, and dropping them, the non-zero contributions to the dipole are given by (see Appendix A)

$$\xi_1(s,d) = 2f\Delta b\frac{s}{d}\left(\Xi_1^{(1)}(s) - \frac{\Xi_2^{(0)}(s)}{5}\right) + \left(\Delta\phi + \frac{5}{2}\Delta v_{\rm g}^2\right) \times\frac{1}{saH}\left(b_{\rm X}b_{\rm Y} + \frac{3}{5}(b_{\rm X}+b_{\rm Y})f + \frac{3}{7}f^2\right)\Xi_1^{(-1)}(s), \tag{3}$$

where the function $f \equiv {\rm d}\ln D/{\rm d}\ln a$ is the linear growth rate, with D being the linear growth factor. We define $\Xi_\ell^{(n)}(s) \equiv \int k^2\,{\rm d}k/(2\pi^2)\,j_\ell(ks)(ks)^{-n}P_{\rm L}(k)$ with j_ℓ and $P_{\rm L}(k)$ being, respectively, the spherical Bessel function and linear matter power spectrum. In equation (3), all terms are proportional to the differential quantities, i.e. $\Delta b \equiv b_{\rm X} - b_{\rm Y}$, $\Delta\phi \equiv \phi_{\rm halo,X} - \phi_{\rm halo,Y}$, and $\Delta v_{\rm g}^2 \equiv v_{\rm g,X}^2 - v_{\rm g,Y}^2$. Accordingly, the non-vanishing dipole arises only when we cross-correlate different biased objects, X $\neq$ Y. To observe the dipole signal and use it as the probe of the LPI test, we preferentially cross-correlate the objects having a similar potential depth, which can be regarded as the conditional average over density fields, δ, for a given potential depth. Hence, a non-zero contribution from, e.g. $\langle\Phi\delta\delta\rangle$, would be present but be small, indeed justified in comparing the analytical predictions with the simulations (Breton et al. 2019).

We note that our model (3) ignores the magnification bias due to the flux-limited galaxy samples that also contributes to the dipole (Bonvin et al. 2014; Hall & Bonvin 2017). As shown in Saga et al. (2022), its impact is small at the scales of interest and hence does not change our results. We keep the Doppler contribution which is also negligible compared to the second term in equation (3) at small scales, but has the comparable amplitude to the magnification bias. If we cross-correlate subhaloes or satellite galaxies, the Doppler contribution may become a non-negligible effect as the Finger-of-God effect, although it has not been appropriately modelled beyond the plane-parallel limit yet, which is beyond the scope of this work.

[1]We ignore the contribution from the linear density field, which could be important to probe the equivalence principle at large scales. However, such a term produces a negligible gravitational redshift at the scales of interest.

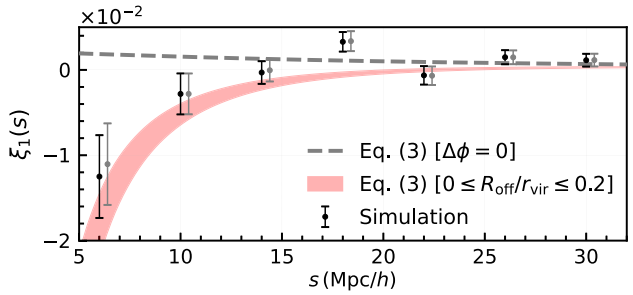

Figure 1. Dipole of the correlation function between different biased objects $(b_X, b_Y) = (2.07, 1.08)$ at $z = 0.33$ whose halo masses correspond to $(M_X, M_Y) = (4.4 \times 10^{13}\,M_\odot/h, 1.6 \times 10^{12}\,M_\odot/h)$ based on the Sheth–Tormen prescription (Sheth & Tormen 1999). The red shaded curve represents the analytical prediction, varying from $R_{off}/r_{vir} = 0$ (lower) to $R_{off}/r_{vir} = 0.2$ (upper), leading to the values of the halo potential $(\phi_{halo,X}, \phi_{halo,Y}) = (-1.6 \times 10^{-5}, -2.9 \times 10^{-6})$ and $(-1.1 \times 10^{-5}, -1.7 \times 10^{-6})$, respectively, while the grey dashed line ignores the halo potential. As we measure the dipole of halo–halo cross-correlation in simulations, the values of the velocity dispersion in this analytical prediction are provided based on the large-scale coherent motion alone (see Appendix B), whose values are $(v^2_{g,X}, v^2_{g,Y}) = (2.2 \times 10^{-6}, 2.6 \times 10^{-6})$. The circles with errorbars represent the simulation results taking both Doppler and gravitational redshift effects (black) and all relevant relativistic effects (grey, artificially shifted to the rightward direction for presentation purposes), whose errorbars are estimated using the jack-knife method (Saga et al. 2020).

Given the linear matter power spectrum and bias parameters, the remaining pieces to be specified for a quantitative prediction of ξ_1 are ϕ_{halo} and v^2_g, which are modelled by the universal halo density profile, called Navarro–Frenk–White profile (Navarro, Frenk & White 1996). Assuming that its functional form is characterized by halo mass and redshift, the halo potential, ϕ_{halo}, is obtained by solving the Poisson equation, while the velocity dispersion, v^2_g, is computed from the Jeans equation (Saga et al. 2020, 2022). Here, we also add the halo coherent motion to v^2_g according to Zhao, Peacock & Li (2013), Zhu et al. (2017), and Di Dio & Seljak (2019). In predicting the dipole, a crucial aspect is that each of the galaxies to cross-correlate does not strictly reside at the halo centre. The presence of the off-centred galaxies induces two competitive effects, i.e. the diminution of the gravitational redshift and non-vanishing transverse Doppler effects, which systematically change the dipole amplitude. We account for them following Hikage et al. (2013) and Yan et al. (2020), and control their potential impact by introducing the off-centring parameter R_{off}. As a result, we can write the parameter dependence explicitly as $\phi_{halo,X}(z, M_X, R_{off,X})$ and $v^2_{g,X}(z, M_X, R_{off,X})$ (see Appendix B).

Putting all ingredients together, we show the analytical prediction of the dipole at $z = 0.33$ in Fig. 1, together with the measured dipole in simulations incorporating longitudinal Doppler and gravitational redshift effects (black circles), and all the relevant relativistic effects (grey circles, Breton et al. 2019). Comparing black with grey circles, the longitudinal Doppler and gravitational redshift effects are shown to be the major contributors to the dipole. Accordingly, it justifies the underlying assumption in our model given in equation (3). In this figure, we vary the off-centring parameter by the typical range for the simulations, i.e. the offset of the deepest potential well from the centre of mass position which is the actual halo position defined in simulations: $0 \le R_{off}/r_{vir} \le 0.2$ (see e.g. Yan et al. 2020). Within the statistical error, the prediction (red curve) describes the simulation results remarkably well down to $5\,h^{-1}$ Mpc, while the prediction ignoring the halo potential (grey dashed) fails to reproduce the negative dipole at small scales. This suggests that the measurements of the dipole, having particularly a negative amplitude at $s \lesssim 30\,h^{-1}$ Mpc, provide us with information about the gravitational redshift effect from the halo potential, and we can use it to test the LPI violation, as we will see below.

3 TEST OF LOCAL POSITION INVARIANCE

Having confirmed that the analytical predictions properly describe the dipole at the scales of our interest, we next quantitatively consider the prospects for constraining the LPI-violation parameter α in equation (1) from upcoming galaxy surveys.

To this end, we perform the Fisher matrix analysis involving several parameters together with α as follows:

(i) *Cosmological parameters*: We assume that the cosmological parameters that characterize the linear matter spectrum P_L and growth of structure are determined by other cosmological probes e.g. cosmic microwave background (CMB) observations, and fix their fiducial values to the seven-year *Wilkinson Microwave Anisotropy Probe (WMAP)* results (Komatsu et al. 2011).

(ii) *Bias parameter*: The redshift-space distortions and baryon acoustic oscillations measurements provide the constraint on $b\sigma_8$ with σ_8 being the fluctuation amplitude smoothed at $8\,h^{-1}$ Mpc. Combining the accurate CMB measurement for power spectrum normalization, we thus have the bias b with a certain error, σ_b (see e.g. Seo & Eisenstein 2003; Taruya, Saito & Nishimichi 2011). We obtain the error by performing another Fisher analysis for these observations (see Appendix C in detail).

On top of these parameters that can be determined independently of the dipole, our theoretical template based on equation (3) involves parameters associated with the properties of haloes for a given redshift:

(i) *Off-centring parameter* R_{off}: In principle, we can determine this parameter separately and accurately from the even multipoles (e.g. Hikage et al. 2013). Here, we set the typical value, $0.2r_{vir}$, as a fiducial value, and impose a Gaussian prior with the expected errors $\sigma_{R_{off}} = 0.01r_{vir}$, where r_{vir} is the virial radius of haloes (e.g. Lukić et al. 2009; Hikage et al. 2013; Yan et al. 2020).

(ii) *Halo mass*: Given the bias model described by e.g. the Sheth–Tormen prescription (Sheth & Tormen 1999), the halo masses $M_{X/Y}$ are inferred from the bias parameters with errors, $\sigma_M = |\partial M/\partial b|\sigma_b$. We incorporate this error into our analysis as a Gaussian prior. This treatment enables us to break the degeneracy between the LPI-violating parameter, α, and potential difference, $\Delta\phi$ as seen in equation (1). The systematic impact of assuming a specific bias model would be reduced, once we can determine the halo masses by complementary probes, e.g. gravitational lensing measurements.

To sum up, we have five free parameters in the theoretical template, $\boldsymbol{\theta} = \{\alpha, R_{off,X/Y}, \text{and } M_{X/Y}\}$. With the above prescription, the LPI test proposed here is performed consistently under the standard cosmological model.

Let us construct the Fisher matrix. For galaxy samples at the nth redshift slice z_n, it is given by the 5×5 matrix:

$$F_{n,ij} = \sum_{s_{1,2}=s_{min}}^{s_{max}} \frac{\partial\xi_1(s_1, z_n)}{\partial\theta_i} \mathcal{C}^{-1}(s_1, s_2, z_n) \frac{\partial\xi_1(s_2, z_n)}{\partial\theta_j}, \tag{4}$$

with $\mathcal{C}$ being the covariance matrix, which is analytically evaluated by taking only the dominant plane-parallel contributions, ignoring also the non-Gaussian contribution (Bonvin, Hui & Gaztanaga 2016; Hall & Bonvin 2017; Saga et al. 2022). We set the minimum separation

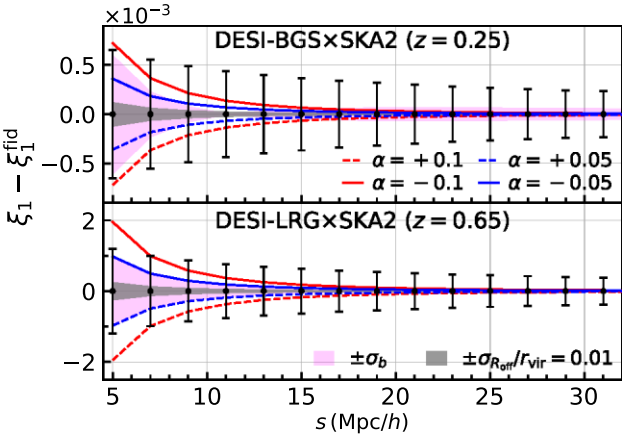

Figure 2. Expected 1σ error on the dipole around the fiducial signal, $(R_{\rm off}/r_{\rm vir}, \alpha) = (0.2, 0)$, for the future surveys as indicated. The red and blue lines represent the difference between the fiducial signal and the one when $\alpha = \pm 0.1$ and ± 0.05, respectively. The grey and magenta regions represent, respectively, the variation of the signal when varying the off-centring parameter and bias parameter within the prior range: $\sigma_{R_{\rm off}}/r_{\rm vir} = 0.01$, $(\sigma_{b,\,\rm DESI\text{-}BGS}, \sigma_{b,\rm SKA2}) = (0.05, 0.02)$ at $z = 0.25$, and $(\sigma_{b,\rm DESI\text{-}LRG}, \sigma_{b,\rm SKA2}) = (0.04, 0.01)$ at $z = 0.65$.

$s_{\rm min}$ to $5\,h^{-1}$ Mpc, above which the analytical prediction reproduces the simulations, and the systematics of baryonic effects would be negligible. We set $s_{\rm max}$ to $30\,h^{-1}$ Mpc, below which the gravitational redshift effect from the halo potential starts to dominate. Adopting a larger $s_{\rm max}$ hardly changes the results. Then, with the inverse Fisher matrix at z_n, $\sigma^2_{n,\alpha} \equiv F^{-1}_{n,\alpha\alpha}$, we combine all the redshift bins by $\sigma_\alpha = 1/\sqrt{\sum_n \sigma^{-2}_{n,\alpha}}$, which gives the expected 1σ error for a given survey on the LPI-violating parameter, marginalizing over other parameters.

Our Fisher matrix analysis considers the cross-correlation function between two distinct galaxy populations obtained from different surveys, assuming that these surveys are maximally overlapped. We examine the combination of the following surveys: Dark energy spectroscopic instrument (DESI) targeting magnitude-limited bright galaxies (BGS), luminous red galaxies (LRGs), and emission line galaxies (ELGs) (Aghamousa et al. 2016), Euclid targeting Hα emitters (Laureijs et al. 2011), Subaru prime focus spectrograph targeting O II ELGs (Takada et al. 2014), and square kilometre array (SKA) targeting H I galaxies with two phases dubbed SKA1 and SKA2 (Bacon et al. 2020; see appendix E of Saga et al. 2022 for the survey parameters). Note that splitting galaxies obtained from a single survey, a cross correlation between two subsamples would also yield a non-zero dipole. However, its detectability strongly depends on how we split the sample (see Saga et al. 2022). In this paper, we rather focus on a solid way that combines two distinct surveys.

Before presenting forecast results, Fig. 2 shows, for illustration, the expected errors around the predicted dipole for DESI-BGS×SKA2 (*top*) and DESI-LRG×SKA2 (*bottom*), with the fiducial set-up (i.e. $R_{\rm off}/r_{\rm vir} = 0.2$ and $\alpha = 0$) at the specific redshifts, $z = 0.25$ and $z = 0.65$, respectively. Here, we also show the expected signals when changing the LPI-violating parameter to $\alpha = \pm 0.1$ and ± 0.05, varying the off-centring parameter within the prior range $\sigma_{R_{\rm off}}/r_{\rm vir} = 0.01$ (grey), and varying the bias parameter within the prior range σ_b derived by performing another Fisher analysis (see Appendix C) as indicated in the caption of the figure (magenta). Fig. 2 suggests that the dipole signal from upcoming surveys

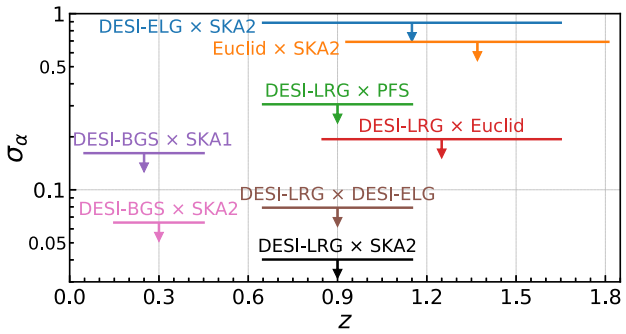

Figure 3. Expected 1σ error on the LPI-violating parameter α, obtained by cross-correlating different sources observed in different surveys as indicated. The length of each horizontal line represents the survey redshift ranges to obtain the 1σ error.

allows us to measure an LPI violation of the order of $\mathcal{O}(\alpha) = 0.01$ even for a single redshift slice if the other parameters are held fixed.

Computing the Fisher matrix, we obtain the 1σ error on the LPI-violating parameter with other parameters marginalized over. Fig. 3 shows the results from various combinations of upcoming surveys against the redshift. Among these, the combination of DESI-LRG and SKA2 gives the tightest constraint with $\sigma_\alpha \approx 0.040$ at $0.7 \lesssim z \lesssim 1.1$. This is attributed to the large bias difference, increasing the signal, and a large number of galaxies in SKA2, reducing the shot noise. Assuming that all the observations shown in Fig. 3 are independent, combining all measurements further improves the constraint on α down to $\sigma_\alpha \approx 0.030$.

The expected upper limit from the proposed LPI test is compared to the previous results for various potential differences $\Delta\phi$, summarized in Fig. 4. In contrast to the previous results, it is worth noting that: (i) the dipole measurement can be a unique probe to explore a new parameter space of the LPI violation, i.e. $\Delta\phi \approx 10^{-5}$, (ii) our method is a new cosmological approach that cannot be categorized as any previous method, and (iii) the method enables us, for the first time, to constrain the LPI violation at cosmological scales.

4 SUMMARY AND DISCUSSION

In this paper, we have explicitly shown that the cross-correlation function between galaxies with different host haloes and clustering bias yields a non-vanishing dipole. Such a feature typically appears at $s \lesssim 30\,h^{-1}$ Mpc, and is dominated by the gravitational redshift effect from the potential of haloes hosting observed galaxies. Analytical predictions combining perturbation theory with halo model prescription agree well with simulations taking the relativistic effects into account. The Fisher matrix analysis based on the analytical model showed that despite the systematics arising from the off-centred galaxies, the dipole measured from the upcoming galaxy surveys offers a unique LPI test at cosmological scales in the high-redshift universe. While the achievable precision of the LPI-violating parameter, $\alpha \lesssim 0.030$, is comparable to the upper limit from the Pound–Rebka–Snider experiments (Pound & Rebka 1959; Pound & Snider 1965) and is weaker than the recent tests based on the null experiments, the proposed method allows us to probe the potential depth of $\Delta\phi \approx 10^{-5}$, which has not been fully explored.

The outcome of our Fisher matrix analysis relies on several simplifications and specific set-ups. Among these, our theoretical template adopts the halo model prescription assuming the one-to-

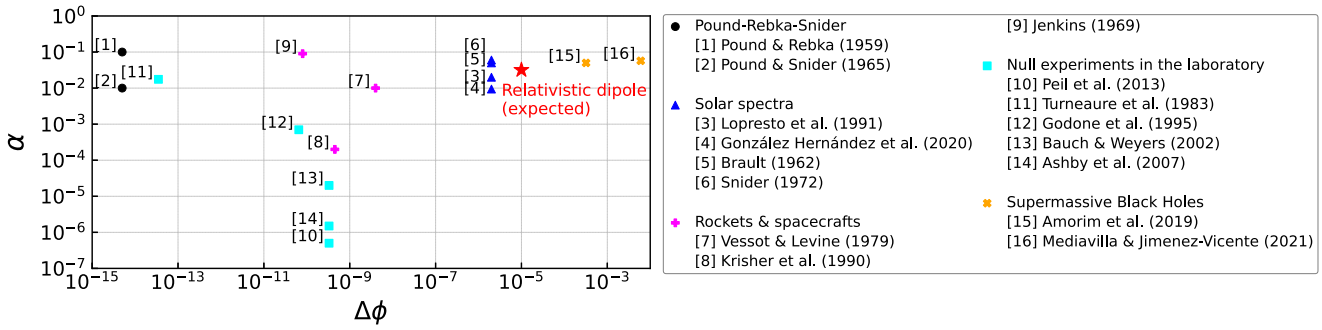

Figure 4. Upper limits on the LPI-violating parameter α as a function of the difference of gravitational potentials by Pound–Rebka–Snider experiments (Pound & Rebka 1959; Pound & Snider 1965), solar spectra measurements (Brault 1962; Snider 1972; Lopresto et al. 1991; González Hernández et al. 2020), rockets and spacecraft experiments (Jenkins 1969; Vessot & Levine 1979; Krisher et al. 1990), null experiments (Turneaure et al. 1983; Godone, Novero & Tavella 1995; Bauch & Weyers 2002; Ashby et al. 2007; Peil et al. 2013), and observations of stars/quasars near the galactic centre supermassive black hole (Amorim et al. 2019; Mediavilla & Jiménez-Vicente 2021) as indicated in the right table. This figure is based on fig. 3 of Amorim et al. (2019), with our forecast result added (indicated by star symbol).

one correspondence between galaxy and halo. Hence, the predicted amplitude of the dipole signal is tightly linked to the halo mass. A more careful modelling based on numerical simulations, though not qualitatively affecting the present results, is required for more precision, taking a proper account of the realistic halo–galaxy connection as well as systematic effects from the assembly bias characterizing the secondary halo properties (Gao, Springel & White 2005; Croton, Gao & White 2007), velocity bias (Baldauf, Desjacques & Seljak 2015; Matsubara 2019), or different properties between infalling and outward moving galaxies implied by quenching (e.g. Bekki et al. 2005; Werle et al. 2022). Modelling them is a common challenge when investigating galaxy–galaxy correlations, for which we need a certain model refined by hydrodynamic simulations, and is therefore beyond the scope of this work. However, once the model including the above systematic effects have been developed, our proposed methodology is still available.

Finally, we quantitatively discuss below that meaningful constraints are still possible in more conservative situations. First, we consider the impact of off-centred galaxies. While our set-up of the off-centring parameter and its Gaussian prior is reasonable for LRGs, upcoming surveys will also observe ELGs, whose properties might not necessarily be the same. Nevertheless, even with a conservative choice of $R_{\rm off}/r_{\rm vir} = 0.4$ and a weak prior condition $\sigma_{R_{\rm off}}/r_{\rm vir} = 0.1$, the degradation of the constraint on α is found to be moderate, and we can still perform a meaningful test from future surveys, with the LPI-violation parameter constrained to be $\sigma_\alpha \approx 0.041$. Secondly, we further take 10 per cent uncertainty in γ, which roughly corresponds to the typical variation range of the spectral index for the galaxy spectral energy distributions (Kaiser 2013) into account in the Fisher analysis, and found the result does not significantly change ($\sigma_\alpha \approx 0.032$). Thirdly, we further examined how the uncertainty in the bias parameter affects the derived constraints on α. We perform the same analysis again for the more conservative case by setting the uncertainty in the bias parameter to twice the fiducial value. Then, we again found that the result does not significantly change ($\sigma_\alpha \approx 0.034$).

Since our method provides a consistency test under general relativity, a non-zero detection of the LPI-violating parameter does not simply imply LPI violation, which is generally inherent in the LPI test. However, we can generalize our methodology to modified gravity, requiring a more systematic and elaborate study, which is beyond the scope of this paper. A pursuit of measuring the dipole signal is indispensable, and the present method will pave a pathway to the cosmological LPI test in the distant universe.

ACKNOWLEDGEMENTS

This work was initiated during the invitation program of JSPS Grant No. L16519. Numerical simulation was granted access to HPC resources of TGCC through allocations made by GENCI (Grand Equipment National de Calcul Intensif) under the allocations A0030402287, A0050402287, A0070402287, and A0090402287. Numerical computation was also carried out partly at the Yukawa Institute Computer Facility. This work was supported by Grant-in-Aid for JSPS Fellows No. 17J10553 (SS) and in part by MEXT/JSPS KAKENHI Grant Numbers JP17H06359, JP20H05861, and 21H01081 (AT). AT also acknowledges the support from JST AIP Acceleration Research Grant No. JP20317829, Japan. SS acknowledges the support from Yukawa Institute for Theoretical Physics (YITP) at Kyoto University, where this work was completed during the visiting program. Also, discussions during the workshop YITP-T-21-06 on "Galaxy shape statistics and cosmology" were useful to complete this work.

DATA AVAILABILITY

The data underlying this article are available in the article.

REFERENCES

Aghamousa A., et al., 2016, preprint (arXiv:1611.00036)
Alam S., Zhu H., Croft R. A. C., Ho S., Giusarma E., Schneider D. P., 2017, MNRAS, 470, 2822
Alcock C., Paczynski B., 1979, Nature, 281, 358
Amorim A., et al., 2019, Phys. Rev. Lett., 122, 101102
Ashby N., Heavner T. P., Jefferts S. R., Parker T. E., Radnaev A. G., Dudin Y. O., 2007, Phys. Rev. Lett., 98, 070802
Bacon D. J., et al., 2020, PASA, 37, e007
Baldauf T., Desjacques V., Seljak U., 2015, Phys. Rev. D, 92, 123507
Bardeen J. M., Bond J. R., Kaiser N., Szalay A. S., 1986, ApJ, 304, 15
Bauch A., Weyers S., 2002, Phys. Rev. D, 65, 081101
Bekki K., Couch W. J., Shioya Y., Vazdekis A., 2005, MNRAS, 359, 949
Bertacca D., Maartens R., Clarkson C., 2014, J. Cosmol. Astropart. Phys., 2014, 013
Beutler F., Di Dio E., 2020, J. Cosmol. Astropart. Phys., 2020, 048
Bonvin C., Durrer R., 2011, Phys. Rev. D, 84, 063505

Bonvin C., Fleury P., 2018, J. Cosmol. Astropart. Phys., 2018, 061
Bonvin C., Hui L., Gaztañaga E., 2014, Phys. Rev. D, 89, 083535
Bonvin C., Hui L., Gaztanaga E., 2016, J. Cosmol. Astropart. Phys., 2016, 021
Bonvin C., Oliveira Franco F., Fleury P., 2020, J. Cosmol. Astropart. Phys., 2020, 004
Brault J. W., 1962, PhD thesis, Univ. Princeton.
Breton M.-A., Rasera Y., Taruya A., Lacombe O., Saga S., 2019, MNRAS, 483, 2671
Bryan G. L., Norman M. L., 1998, ApJ, 495, 80
Bullock J. S., Kolatt T. S., Sigad Y., Somerville R. S., Kravtsov A. V., Klypin A. A., Primack J. R., Dekel A., 2001, MNRAS, 321, 559
Cai Y.-C., Kaiser N., Cole S., Frenk C., 2017, MNRAS, 468, 1981
Challinor A., Lewis A., 2011, Phys. Rev. D, 84, 043516
Cooray A., Sheth R., 2002, Phys. Rep., 372, 1
Croft R. A. C., 2013, MNRAS, 434, 3008
Croton D. J., Gao L., White S. D. M., 2007, MNRAS, 374, 1303
Dai D.-C., Li Z., Stojkovic D., 2019, ApJ, 871, 119
Di Dio E., Seljak U., 2019, J. Cosmol. Astropart. Phys., 2019, 050
Di Dio E., Durrer R., Marozzi G., Montanari F., 2014, J. Cosmol. Astropart. Phys., 2014, 017
Gao L., Springel V., White S. D. M., 2005, MNRAS, 363, L66
Godone A., Novero C., Tavella P., 1995, Phys. Rev. D, 51, 319
González Hernández J. I. et al., 2020, A&A, 643, A146
Hall A., Bonvin C., 2017, Phys. Rev. D, 95, 043530
Hamilton A. J. S., 1992, ApJ, 385, L5
Hikage C., Mandelbaum R., Takada M., Spergel D. N., 2013, MNRAS, 435, 2345
Jenkins R. E., 1969, AJ, 74, 960
Jimeno P., Broadhurst T., Coupon J., Umetsu K., Lazkoz R., 2015, MNRAS, 448, 1999
Kaiser N., 1987, MNRAS, 227, 1
Kaiser N., 2013, MNRAS, 435, 1278
Komatsu E. et al., 2011, ApJS, 192, 18
Krisher T. P., Anderson J. D., Campbell J. K., 1990, Phys. Rev. Lett., 64, 1322
Laureijs R., et al., 2011, preprint (arXiv:1110.3193)
Leefer N., Weber C. T. M., Cingöz A., Torgerson J. R., Budker D., 2013, Phys. Rev. Lett., 111, 060801
Łokas E. L., Mamon G. A., 2001, MNRAS, 321, 155
Lopresto J. C., Schrader C., Pierce A. K., 1991, ApJ, 376, 757
Lukić Z., Reed D., Habib S., Heitmann K., 2009, ApJ, 692, 217
Matsubara T., 2000, ApJ, 537, L77
Matsubara T., 2019, Phys. Rev. D, 100, 083504
McDonald P., 2009, J. Cosmol. Astropart. Phys., 2009, 026
Mediavilla E., Jiménez-Vicente J., 2021, ApJ, 914, 112
Moschella M., Slone O., Dror J. A., Cantiello M., Perets H. B., 2022, MNRAS, 514, 1071
Mpetha C. T. et al., 2021, MNRAS, 503, 669
Navarro J. F., Frenk C. S., White S. D. M., 1996, ApJ, 462, 563
Novikov E. A., 1969, Sov. J. Exp. Theor. Phys., 30, 512
Peil S., Crane S., Hanssen J. L., Swanson T. B., Ekstrom C. R., 2013, Phys. Rev. A, 87, 010102
Pound R. V., Rebka G. A., 1959, Phys. Rev. Lett., 3, 439
Pound R. V., Snider J. L., 1965, Phys. Rev., 140, 788
Sadeh I., Feng L. L., Lahav O., 2015, Phys. Rev. Lett., 114, 071103
Saga S., Taruya A., Breton M.-A., Rasera Y., 2020, MNRAS, 498, 981
Saga S., Taruya A., Rasera Y., Breton M.-A., 2022, MNRAS, 511, 2732
Sasaki M., 1987, MNRAS, 228, 653
Seo H.-J., Eisenstein D. J., 2003, ApJ, 598, 720
Shandarin S. F., Zeldovich Y. B., 1989, Rev. Mod. Phys., 61, 185
Sheth R. K., Diaferio A., 2001, MNRAS, 322, 901
Sheth R. K., Tormen G., 1999, MNRAS, 308, 119
Snider J. L., 1972, Phys. Rev. Lett., 28, 853
Takada M. et al., 2014, PASJ, 66, R1
Tansella V., Bonvin C., Durrer R., Ghosh B., Sellentin E., 2018, J. Cosmol. Astropart. Phys., 2018, 019
Taruya A., Okumura T., 2020, ApJ, 891, L42
Taruya A., Saito S., Nishimichi T., 2011, Phys. Rev. D, 83, 103527
Taruya A., Saga S., Breton M.-A., Rasera Y., Fujita T., 2020, MNRAS, 491, 4162
Turneaure J. P., Will C. M., Farrell B. F., Mattison E. M., Vessot R. F. C., 1983, Phys. Rev. D, 27, 1705
Vessot R. F. C., Levine M. W., 1979, Gen. Relativ. Gravit. 10, 181
Vessot R. F. C. et al., 1980, Phys. Rev. Lett., 45, 2081
Werle A. et al., 2022, ApJ, 930, 43
Will C. M., 2018, Theory and Experiment in Gravitational Physics, 2 edn. Cambridge Univ. Press, Cambridge
Wojtak R., Hansen S. H., Hjorth J., 2011, Nature, 477, 567
Yan Z., Raza N., Van Waerbeke L., Mead A. J., McCarthy I. G., Tröster T., Hinshaw G., 2020, MNRAS, 493, 1120
Yoo J., 2010, Phys. Rev. D, 82, 083508
Yoo J., 2014, Class. Quantum Gravity, 31, 234001
Yoo J., Zaldarriaga M., 2014, Phys. Rev. D, 90, 023513
Zel'dovich Y. B., 1970, A&A, 5, 84
Zhao H., Peacock J. A., Li B., 2013, Phys. Rev. D, 88, 043013
Zhu H., Alam S., Croft R. A. C., Ho S., Giusarma E., 2017, MNRAS, 471, 2345

APPENDIX A: DERIVATION OF EQUATION (3)

We present the derivation of the analytical model for the dipole cross-correlation function given at equation (3). This derivation builds on our previous works (Saga et al. 2020, 2022), but we here succinctly summarize our treatment and the approximation, which enable us to compute the dipole cross-correlation with one-dimensional numerical integration. After presenting a rigorous expression for the observed density field based on the Zel'dovich approximation in Appendix A1, a simplified expression is derived in Appendix A2, leading to an analytical model of the dipole cross-correlation involving only the one-dimensional integrals.

A1 Preliminary

Our starting point is a mapping relation between the real and redshift space given at equation (2) in the main text, which includes the standard Doppler effect, the gravitational redshift effect due to the non-linear halo potential, and contributions arising from the velocity dispersions. In what follows, we denote the relativistic effects, except the standard Doppler term, by $\epsilon_{\rm NL}$. Equation (2) is then rewritten with

$$\boldsymbol{s} = \boldsymbol{x} + \frac{1}{aH}\left(\boldsymbol{v}\cdot\hat{\boldsymbol{x}}\right)\hat{\boldsymbol{x}} + \epsilon_{\rm NL}\hat{\boldsymbol{x}}, \tag{A1}$$

$$\epsilon_{\rm NL} = -\frac{1}{aH}\left(\phi_{\rm halo} - \gamma v_{\rm g}^2\right), \tag{A2}$$

where $\phi_{\rm halo}$ and $v_{\rm g}^2$ stand for, respectively, the gravitational potential of haloes and velocity dispersions, whose explicit modelling is presented in Appendix B. In equation (A2), the first and second terms in the right-hand side express the gravitational redshift effect arising from the deep halo potential and the sum of the transverse Doppler, light-cone, and surface brightness modulation effects mainly due to the velocity dispersions of galaxies, which are the first and second major contributions to the small-scale dipole signal, respectively (Breton et al. 2019). Note that we set $\gamma = -5/2$ as a fiducial value, taken from Kaiser (2013). Here, the quantity $\epsilon_{\rm NL}$ is described by the non-perturbative contribution due to the non-linearies of the halo/galaxy formation and evolution.

In measuring the dipole cross-correlation between different types of galaxies, we are particularly interested in a pair of galaxy samples, each of which resides at similar halos having mostly the same value of $\epsilon_{\rm NL}$. This correlation can be regarded as the conditional

average over the halo density field for a fixed $\epsilon_{\rm NL}$. Hence, we treat the quantity $\epsilon_{\rm NL}$ not as a random variable but as a constant value which depends on the halo mass and redshift. Although a more general expression of the mapping relation discussed in the literature involves contributions from the integrated Sachs-Wolfe and Shapiro time-delay effects (e.g. Yoo 2010; Bonvin & Durrer 2011; Challinor & Lewis 2011), we retain relevant contributions in $\epsilon_{\rm NL}$ to the scales of our interest, $\lesssim 30\,h^{-1}$ Mpc (Breton et al. 2019; Saga et al. 2020).

Following our previous works (Saga et al. 2020; Taruya et al. 2020), we adopt the Zel'dovich approximation, known as the first-order Lagrangian perturbation theory (Novikov 1969; Zel'dovich 1970; Shandarin & Zeldovich 1989), in order, which provides a simple way to deal with redshift-space distortions involving the wide-angle effect even beyond linear regime. The building block in Lagrangian perturbation theory is a displacement field, which relates the Eulerian position, $\boldsymbol{x}$, to the Lagrangian position (initial position), $\boldsymbol{q}$, at the time of interest. Denoting the displacement field in the Zel'dovich approximation by $\boldsymbol{\Psi}(\boldsymbol{q},t)$, which is related to the Lagrangian linear density field $\delta_{\rm L}(\boldsymbol{q},t)$ through $\nabla\cdot\boldsymbol{\Psi}(\boldsymbol{q},t)=-\delta_{\rm L}(\boldsymbol{q},t)$, and assuming that the objects of our interest follow the velocity flow of mass distributions (no velocity bias), we express the Eulerian position $\boldsymbol{x}$ and velocity field $\boldsymbol{v}$ as

$$\boldsymbol{x}(\boldsymbol{q},t)=\boldsymbol{q}+\boldsymbol{\Psi}(\boldsymbol{q},t), \tag{A3}$$

$$\boldsymbol{v}(\boldsymbol{q},t)=a\frac{{\rm d}\boldsymbol{\Psi}(\boldsymbol{q},t)}{{\rm d}t}=aHf\boldsymbol{\Psi}(\boldsymbol{q},t), \tag{A4}$$

where we define the linear growth rate by $f\equiv{\rm dln}\,D_+(a)/{\rm dln}\,a$ with $D_+(t)$ being the linear growth factor. The second equality is valid in the Zel'dovich approximation, where the time dependence of the displacement field is solely encapsulated in the factor $D_+(t)$, i.e. $\boldsymbol{\Psi}\propto D_+(t)$.

Substituting eqs.(A3) and (A4) into equation (A1), the relation between the redshift-space position, $\boldsymbol{s}$, and the Lagrangian position, $\boldsymbol{q}$, becomes

$$\begin{aligned} s_i &= q_i+\left(\delta_{ij}+f\,\hat{x}_i\hat{x}_j\right)\Psi_i(\boldsymbol{q})+\epsilon(\boldsymbol{x})\hat{x}_i \\ &\simeq q_i+R_{ij}(\hat{\boldsymbol{q}})\Psi_j(\boldsymbol{q})+\epsilon(\boldsymbol{q})\hat{q}_i, \end{aligned} \tag{A5}$$

where we define $R_{ij}(\hat{\boldsymbol{q}})\equiv\delta_{ij}+f\hat{q}_i\hat{q}_j$. Here and hereafter, we use the Einstein summation convention. Note that the second line is valid in the Zel'dovich approximation.

Using the number conservation between Lagrangian space and redshift space, we express the number density of the biased objects X in redshift space, $n_{\rm X}^{\rm (S)}(\boldsymbol{s})$, in terms of the Lagrangian space quantities through equation (A5):

$$\begin{aligned} n_{\rm X}^{\rm (S)}(\boldsymbol{s}) &= \bar{n}_{\rm X}\left(1+b_{\rm X}^{\rm L}\delta_{\rm L}(\boldsymbol{q})\right)\left|\frac{\partial s_i}{\partial q_j}\right|^{-1} \\ &= \bar{n}_{\rm X}\int{\rm d}^3\boldsymbol{q}\,\left(1+b_{\rm X}^{\rm L}\delta_{\rm L}(\boldsymbol{q})\right)\delta_{\rm D}(s_i-q_i-R_{ij}\Psi_j+\epsilon\hat{q}_i) \\ &= \bar{n}_{\rm X}\int{\rm d}^3\boldsymbol{q}\int\frac{{\rm d}^3\boldsymbol{k}}{(2\pi)^3}\,{\rm e}^{{\rm i}k_i\left(s_i-q_i-R_{ij}\Psi_j-\epsilon\hat{q}_i\right)}\left(1+b_{\rm X}^{\rm L}\delta_{\rm L}(\boldsymbol{q})\right). \end{aligned} \tag{A6}$$

Here, we assume the linear galaxy bias, and the quantity $b_{\rm X}^{\rm L}$ is the Lagrangian linear bias parameter of the biased objects X, whichis related to the Eulerian bias $b_{\rm X}$ through $b_{\rm X}=1+b_{\rm X}^{\rm L}$. The quantity $\bar{n}_{\rm X}$ is the mean number density of the biased objects X at a given redshift.

Provided the number density, the density fluctuation $\delta_{\rm X}^{\rm (S)}$ is defined as follows:

$$\delta_{\rm X}^{\rm (S)}(\boldsymbol{s})\equiv\frac{n_{\rm X}^{\rm (S)}(\boldsymbol{s})}{\left\langle n_{\rm X}^{\rm (S)}(\boldsymbol{s})\right\rangle}-1, \tag{A7}$$

where the bracket $\langle\cdots\rangle$ stands for the ensemble average. We note that the quantity $\langle n_{\rm X}^{\rm (S)}\rangle$ differs from $\bar{n}_{\rm X}$, due to the directional-dependence $\hat{\boldsymbol{q}}$ in $R_{ij}(\hat{\boldsymbol{q}})$ and $\epsilon(\boldsymbol{q})\hat{\boldsymbol{q}}$ (see Saga et al. 2020; Taruya et al. 2020).

With the definition given by equation (A7), an analytical expression of the correlation function is regorously derived in Saga et al. (2020), without invoking other approximations except the Zel'dovich approximation under the Gaussianity of the linear density field $\delta_{\rm L}$ and linear galaxy bias (see eqs. 3.14– 3.18 in their paper).

A2 Analytical model of dipole cross-correlation

Here, we derive a simplied analytical expression of dipole cross correlation function, following Saga et al. (2022). First, we linearize the expression at equation (A7) with respect to the displacement field. Taruya et al. (2020) showed that this treatment still gives an accurate description of the dipole cross-correlation function at the scales of our interest. On top of this, we also expand the term proportional to $\epsilon_{\rm NL}$ from the exponent, which are supposed to be small though the term involves non-perturbative contributions. Then, we obtain

$$\begin{aligned} \delta^{\rm (S)}(\boldsymbol{s}) = \int{\rm d}^3\boldsymbol{q}\int\frac{{\rm d}^3\boldsymbol{k}}{(2\pi)^3}\,{\rm e}^{{\rm i}\boldsymbol{k}\cdot(\boldsymbol{s}-\boldsymbol{q})}\Big[&b^{\rm L}\delta_{\rm L}-{\rm i}k_iR_{ij}\Psi_j \\ &+\epsilon_{\rm NL}\left(-({\rm i}\boldsymbol{k}\cdot\hat{\boldsymbol{q}})+\frac{2}{s}\right)\left(b^{\rm L}\delta_{\rm L}-{\rm i}k_iR_{ij}\Psi_j\right)\Big], \end{aligned} \tag{A8}$$

where the first line consists of the the real-space contribution and standard Doppler term, while the second line stands for the leading-order contribtions of the non-perturbative relativistic correction.

Now we define the correlation function between the populations X at $\boldsymbol{s}_1$ and Y at $\boldsymbol{s}_2$:

$$\xi(\boldsymbol{s}_1,\boldsymbol{s}_2)\equiv\left\langle\delta_{\rm X}^{\rm (S)}(\boldsymbol{s}_1)\delta_{\rm Y}^{\rm (S)}(\boldsymbol{s}_2)\right\rangle. \tag{A9}$$

Substituting equation (A8) into equation (A9), and performing the $\boldsymbol{q}$-integrals, we obtain the expression for the cross-correlation function (Saga et al. 2022):

$$\xi(\boldsymbol{s}_1,\boldsymbol{s}_2)=\int\frac{{\rm d}^3k}{(2\pi)^3}{\rm e}^{{\rm i}\boldsymbol{k}\cdot\boldsymbol{s}}P_{\rm L}(k) \tag{A10}$$

$$\begin{aligned} &\times\Bigg[\left(b_{\rm X}+f\mu_{k1}^2+{\rm i}f\frac{2}{ks_1}\mu_{k1}\right)\left(b_{\rm Y}+f\mu_{k2}^2-{\rm i}f\frac{2}{ks_2}\mu_{k2}\right) \\ &+\frac{\epsilon_{\rm NL,X}}{s_1}\Bigg(-1+\mu_{k1}^2+{\rm i}f\frac{2}{ks_1}\mu_{k1}+{\rm i}b_{\rm X}ks_1\mu_{k1} \\ &-2f\mu_{k1}^2+{\rm i}\frac{2}{ks_1}\mu_{k1}+{\rm i}fks_1\mu_{k1}^3\Bigg)\left(b_{\rm Y}+f\mu_{k2}^2-{\rm i}f\frac{2}{ks_2}\mu_{k2}\right) \\ &+\frac{\epsilon_{\rm NL,Y}}{s_2}\Bigg(-1+\mu_{k2}^2-{\rm i}f\frac{2}{ks_2}\mu_{k2}-{\rm i}b_{\rm Y}ks_2\mu_{k2}-2f\mu_{k2}^2 \\ &-{\rm i}\frac{2}{ks_2}\mu_{k2}-{\rm i}fks_2\mu_{k2}^3\Bigg)\left(b_{\rm X}+f\mu_{k1}^2+{\rm i}f\frac{2}{ks_1}\mu_{k1}\right)\Bigg], \end{aligned} \tag{A11}$$

where we define $\mu_{k1}=\hat{\boldsymbol{s}}_1\cdot\hat{\boldsymbol{k}}$ and $\mu_{k2}=\hat{\boldsymbol{s}}_2\cdot\hat{\boldsymbol{k}}$. The function $P_{\rm L}(k)$ stands for the linear power spectrum of the density field $\delta_{\rm L}$ given by

$$\left\langle\delta_{\rm L}(\boldsymbol{k})\delta_{\rm L}(\boldsymbol{k}')\right\rangle=(2\pi)^3\delta_{\rm D}(\boldsymbol{k}+\boldsymbol{k}')P_{\rm L}(k). \tag{A12}$$

In equation (A11), introducing a polar coordinate system in $\boldsymbol{k}$, the integral over the azimuthal angle performed analytically using

the formulae given in appendix A in Saga et al. (2022). Then, the dependence of the correlation function on the vectors $\boldsymbol{s}_1$ and $\boldsymbol{s}_2$ in equation (A11) is described by only the following quantities: $(\hat{\boldsymbol{s}}\cdot\hat{\boldsymbol{s}}_1)$, $(\hat{\boldsymbol{s}}\cdot\hat{\boldsymbol{s}}_2)$, $(\hat{\boldsymbol{s}}_1\cdot\hat{\boldsymbol{s}}_2)$, s_1, and s_2. These quantities can be rewritten in terms of the following three variables, i.e. separation $s=|\boldsymbol{s}_2-\boldsymbol{s}_1|$, the line-of-sight distance $d=|\boldsymbol{s}_1+\boldsymbol{s}_2|/2$, and directional cosine $\mu=\hat{\boldsymbol{s}}\cdot\hat{\boldsymbol{d}}$. Since we are interested in the cases with $s\ll d$, we can expand the quantities as

$$s_{1,2}\simeq d\left(1\mp\frac{1}{2}\frac{s}{d}\mu\right),\quad \hat{\boldsymbol{s}}\cdot\hat{\boldsymbol{s}}_{1,2}\simeq\mu\mp\frac{1}{2}(1-\mu^2)\frac{s}{d},\hat{\boldsymbol{s}}_1\cdot\hat{\boldsymbol{s}}_2\simeq 1, \tag{A13}$$

with $-$ for $\boldsymbol{s}_1$ and $+$ for $\boldsymbol{s}_2$, and these relations are valid at $\mathcal{O}(s/d)$. Then, the resultant expression is given as a polynomial form of μ. After performing the multipole expansion of ξ in terms of μ:

$$\xi_1(s,d)=\frac{3}{2}\int_{-1}^{1}\mathrm{d}\mu\,\xi_{\rm XY}(s,d,\mu)\,\mu, \tag{A14}$$

we arrive straightforwardly at equation (3) in the main text:

$$\begin{aligned}\xi_1(s,d)=&\,2f\Delta b\frac{s}{d}\left(\Xi_1^{(1)}(s)-\frac{\Xi_2^{(0)}(s)}{5}\right)\\&-\frac{\Delta\epsilon_{\rm NL}}{saH}\left(b_{\rm X}b_{\rm Y}+\frac{3}{5}(b_{\rm X}+b_{\rm Y})f+\frac{3}{7}f^2\right)\Xi_1^{(-1)}(s),\end{aligned} \tag{A15}$$

where $\Delta b=b_{\rm X}-b_{\rm Y}$ and $\Delta\epsilon_{\rm NL}=\epsilon_{\rm NL,X}-\epsilon_{\rm NL,Y}$, and we define

$$\Xi_\ell^{(n)}(s)=\int\frac{k^2\mathrm{d}k}{2\pi^2}\frac{j_\ell(ks)}{(ks)^n}P_{\rm L}(k). \tag{A16}$$

In equation (A15), the first and second lines are, respectively, proportional to $\delta_{\rm L}^2$ and $\phi_{\rm halo,X/Y}\delta_{\rm L}^2$ or $v_{\rm g,X/Y}^2\delta_{\rm L}^2$. This dependence comes from the fact the we retain the most dominant leading-order contribution to reproduce the prediction by the exact expression. Hence, equation (A15) is still relevant to describe major relativistic effects, similar to those involving a more intricate second-order expressions in perturbation theory (e.g. Bertacca, Maartens & Clarkson 2014; Di Dio et al. 2014; Yoo & Zaldarriaga 2014).

It has been shown in Saga et al. (2022) that the dipole cross-correlation based on a rigorous calculation of equations (A6) and (A7) (eqs. 3.14–3.18 of their paper) agrees very well with the prediction by equation (A15), even down to $s\approx 5\,h^{-1}$ Mpc. This ensures that an accurate calculation of Fisher matrix is possible with the model given by equation (A15), allowing systematic investigations with less computationally cost.

APPENDIX B: MODEL OF THE NON-PERTURBATIVE TERMS

Here, we present the model of the non-perturbative term in equation (A2). The non-perturbative term contains two contributions. One is the gravitational redshift effect due to the gravitational potential of haloes and another is the contribution from the velocity dispersion of galaxies, which are presented in Appendices B1 and B2, respectively.

B1 Halo gravitational potential

Based on the the universal halo density profile called Navarro−Frenk–White (NFW) profile (Navarro et al. 1996) and its gravitational potential, we present an analytical model for the non-perturbative halo potential, $\phi_{\rm halo}$, given in equation (A2). The NFW profile quantitatively describes the halo density profiles in cosmological N-body simulations, given by

$$\rho_{\rm NFW}(r,z,M)=\frac{\rho_{\rm s}(z,M)}{(r/r_{\rm s}(z,M))\{1+(r/r_{\rm s}(z,M))\}^2}, \tag{B1}$$

with r, z, and M being radius from the halo centre, redshift, and halo mass, respectively. The overdensity, $\rho_{\rm s}(z,M)$, and the scale radius, $r_{\rm s}(z,M)$, are related to the concentration parameter $c_{\rm vir}$ through

$$\begin{aligned}\rho_{\rm s}(z,M)=&\,\frac{\Delta_{\rm vir}(z)\rho_{\rm m0}}{3}c_{\rm vir}^3(M,z)\\&\times\left[\ln(1+c_{\rm vir}(z,M))-\frac{c_{\rm vir}(z,M)}{1+c_{\rm vir}(z,M)}\right]^{-1},\end{aligned} \tag{B2}$$

$$r_{\rm s}(z,M)=\frac{r_{\rm vir}(z,M)}{c_{\rm vir}(z,M)}, \tag{B3}$$

where we define the virial radius $r_{\rm vir}$ and virial overdensity $\Delta_{\rm vir}$ by (Bryan & Norman 1998; Bullock et al. 2001)

$$r_{\rm vir}(z,M)=\left(\frac{3M}{4\pi\Delta_{\rm vir}(z)\rho_{\rm m0}}\right)^{\frac{1}{3}}, \tag{B4}$$

$$\Delta_{\rm vir}(z)=\frac{18\pi^2+82\,(\Omega_{\rm m}(z)-1)-39\,(\Omega_{\rm m}(z)-1)^2}{\Omega_{\rm m}(z)}, \tag{B5}$$

$$\Omega_{\rm m}(z)=\frac{(1+z)^3\Omega_{\rm m0}}{(1+z)^3\Omega_{\rm m0}+\Omega_{\Lambda0}}. \tag{B6}$$

We use the following fitting form for the concentration parameter (Bullock et al. 2001; Cooray & Sheth 2002):

$$c_{\rm vir}(z,M)=\frac{9}{1+z}\left(\frac{M}{M_*(z)}\right)^{-0.13}, \tag{B7}$$

where $M_*(z)$ stands for the characteristic mass scale defined by $\sigma_M(M_*)D_+(z)=\delta_{\rm crit}$. The quantity $\delta_{\rm crit}$ is the critical over-density of the spherical collapse model, and σ_M is the root-mean square amplitude of the matter density fluctuations smoothed with top-hat filter of the radius $R=(3M/(4\pi\overline{\rho}))^{1/3}$ with $\overline{\rho}$ being the mean mass density.

Solving the Poisson equation, we obtain the gravitational potential of the NFW profile at equation (B1) under the boundary condition $\phi_{\rm NFW}\to 0$ at $r\to\infty$:

$$\begin{aligned}\phi_{\rm NFW}(r,z,M)=&-4\pi G(1+z)\rho_{\rm s}(z,M)r_{\rm s}^2(z,M)\\&\times\left(\frac{r}{r_{\rm s}(z,M)}\right)^{-1}\ln\left(1+\frac{r}{r_{\rm s}(z,M)}\right).\end{aligned} \tag{B8}$$

To incorporate the impact from the off-centered galaxy position into the potential estimate, we introduce the probability distribution function of the galaxy position inside each halo, $p_{\rm off}$, normalized as follows (Hikage et al. 2013):

$$\int_0^{r_{\rm vir}}4\pi r^2 p_{\rm off}(r;R_{\rm off})\,\mathrm{d}r=1. \tag{B9}$$

The probability distribution function is assumed to be the Gaussian distribution, i.e. $p_{\rm off}(r;R_{\rm off})\propto\exp(-(r/R_{\rm off})^2/2)$ with $R_{\rm off}$ being the offset parameter. Using the distribution function $p_{\rm off}$, we estimate the halo potential at the off-centered galaxy position by

$$\overline{\phi}_{\rm NFW}(z,M,R_{\rm off})=\int_0^{r_{\rm vir}}4\pi r^2\phi_{\rm NFW}(r,z,M)p_{\rm off}(r;R_{\rm off})\,\mathrm{d}r, \tag{B10}$$

Finally, the averaged NFW potential is adopted as the model $\phi_{\rm halo}$ in equation (A2):

$$\phi_{\rm halo}=\overline{\phi}_{\rm NFW}(z,M,R_{\rm off}). \tag{B11}$$

We note that the off-centering parameter $R_{\rm off}$ can be estimated by using even multipole moments independently of the dipole moment (Hikage et al. 2013).

B2 Velocity dispersions

Next, we consider the velocity dispersion contribution, $v_{\rm g}^2$, in equation (A2), which is expressed as a sum of the two contributions (e.g. Sheth & Diaferio 2001):

$$v^2(r, z, M) = v_{\rm vir}^2(r, z, M) + v_{\rm halo}^2(z, M). \tag{B12}$$

Here, the first and second terms at the right-hand side are originated respectively from the virial motion within a halo and the large-scale coherent motion of the host haloes. The second term, which is a subdominant contribution, is non-vanishing even if the galaxies reside at the centre of the haloes.

To compute the velocity dispersion of the virial motion, $v_{\rm vir}^2$, we adopt the analytical formula for the velocity dispersion of the NFW density profile (see equation 14 of Łokas & Mamon 2001):

$$v_{\rm vir}^2(r, z, M) = \alpha(r, z, M)\frac{GM}{r_{\rm vir}}, \tag{B13}$$

with the function $\alpha(r, z, M)$ given by

$$\begin{aligned}\alpha(r, z, M) = \frac{3}{2}c_{\rm vir}^2 g(c_{\rm vir})x(1+c_{\rm vir}x)^2\Bigg[&6{\rm Li}_2(-c_{\rm vir}x) + \pi^2 - \ln(c_{\rm vir}x) \\ &- \frac{1}{c_{\rm vir}x} - \frac{1}{(1+c_{\rm vir}x)^2} - \frac{6}{1+c_{\rm vir}x} + 3\ln^2(1+c_{\rm vir}x) \\ &+ \ln(1+c_{\rm vir}x)\left(1 + \frac{1}{(c_{\rm vir}x)^2} - \frac{4}{c_{\rm vir}x} - \frac{2}{1+c_{\rm vir}x}\right)\Bigg],\end{aligned} \tag{B14}$$

where the quantity x and function ${\rm Li}_2(x)$ respectively stand for the radius normalized by the virial radius, $x \equiv r/r_{\rm vir}$, and the dilogarithm. The function $g(c_{\rm vir})$ is defined as $g(c_{\rm vir}) \equiv [\ln(1 + c_{\rm vir}) - c_{\rm vir}/(1 + c_{\rm vir})]^{-1}$.

We estimate the velocity dispersion due to the large-scale coherent motion, $v_{\rm halo}^2$, by using the peak theory prediction based on the linear Gaussian density fields (Bardeen et al. 1986; Sheth & Diaferio 2001):

$$v_{\rm halo}^2(z, M) = (aHfD_+)^2\sigma_{-1}^2(M)\left(1 - \frac{\sigma_0^4(M)}{\sigma_1^2(M)\sigma_{-1}^2(M)}\right), \tag{B15}$$

where we define the function σ_n by

$$\sigma_n^2(M) = \int \frac{k^2{\rm d}k}{2\pi^2}\, k^{2n} P_{\rm L}(k) W^2(kR). \tag{B16}$$

Here, the function $W(x) = 3j_1(x)/x$ is the Fourier transform of the real space top-hat window function, and the radius R is related to the halo mass M through $M = 4\pi\bar{\rho}R^3/3$ with $\bar{\rho}$ being the background matter density.

We take the off-centering effect into account the velocity dispersion equation (B12) by the same averaging procedure in equation (B10):

$$\overline{v^2}(z, M, R_{\rm off}) = \int_0^{r_{\rm vir}} 4\pi r^2 v^2(r, z, M) p_{\rm off}(r; R_{\rm off})\, {\rm d}r, \tag{B17}$$

Finally, we adopt the velocity dispersion obtained in this way as the model v_g^2 in equation (A2):

$$v_{\rm g}^2 = \overline{v^2}(z, M, R_{\rm off}). \tag{B18}$$

APPENDIX C: FISHER ANALYSIS FOR UNCERTAINTY IN THE BIAS PARAMETER

In the Fisher analysis for deriving the constraint on α, the uncertainty in halo masses σ_M, inferred from the uncertainty in the bias parameters σ_b, is introduced as a Gaussian prior. We here describe the Fisher analysis for deriving the uncertainty in the bias parameter σ_b in detail.

We consider the observed anisotropies arising only from the standard Doppler effect, which plays a dominant role when constraining the bias parameter b as well as the linear growth rate f and relevant cosmological parameters. This is particularly the case if we use the even multipole moments of the clustering anisotropies at large scales (e.g. Bonvin et al. 2014; Breton et al. 2019), and hence we safely ignore the other relativitsic effects. Taking the plane parallel limit, we have the linear model of the galaxy auto power spectrum in redshift space (Kaiser 1987; Hamilton 1992):

$$P_{\rm gg}(k, \mu_k) = (b + f\mu_k)^2 P_{\rm L}(k), \tag{C1}$$

where we define $\mu_k = \hat{\boldsymbol{k}} \cdot \hat{\boldsymbol{z}}$ with the constant line of sight vector $\hat{\boldsymbol{z}}$. On top of the clustering anisotropy induced by the Doppler effect given in equation (C1), the observed power spectrum in comoving space exhibits additional anisotropies induced by the Alcock–Paczynski effect (Alcock & Paczynski 1979), which is modelled by replacing the projected wavenumbers perpendicular and parallel to the line-of-sight direction, $k_\perp$ and $k_\parallel$ with $(d_{\rm A}/d_{\rm A,\,fid})k_\perp$ and $(H/H_{\rm fid})^{-1}k_\parallel$, respectively, and further by multiplying the factor $(H/H_{\rm fid})(d_{\rm A}/d_{\rm A,fid})^{-2}$ with the power spectrum (see e.g. Seo & Eisenstein 2003; Taruya et al. 2011). Here, we define the angular diameter distance $d_{\rm A}$, and the parameters $H_{\rm fid}$ and $d_{\rm A,fid}$ stand for the quantities calculated in the fiducial cosmological model.

As a result, the power spectrum in the model is characterized by four parameters $\boldsymbol{\theta} = (b, f, H/H_{\rm fid}, d_{\rm A}/d_{\rm A,fid})$. Assuming a flat Λcold dark matter model determined by the seven-year *WMAP* results (Komatsu et al. 2011), we perform the Fishser analysis to derive the parameter constraints given the survey parameters, i.e. the mean redshift slice z, survey volume V, and mean number density of galaxies $n_{\rm g}$. The Fisher matrix is given by (e.g. Taruya & Okumura 2020):

$$\begin{aligned}F_{ij} = \frac{V}{8\pi^2}\int_{k_{\rm min}}^{k_{\rm max}} k^2\,{\rm d}k \int_{-1}^{1}{\rm d}\mu_k \\ \times \frac{\partial P_{\rm gg}(k, \mu_k)}{\partial\theta_i}\frac{\partial P_{\rm gg}(k, \mu_k)}{\partial\theta_j}\left(P_{\rm gg}(k, \mu_k) + n_{\rm g}^{-1}\right)^{-2},\end{aligned} \tag{C2}$$

where the minimum and maximum wavenumbers used in the analysis are set to $k_{\rm min} = 2\pi\, V^{-1/3}$ and $k_{\rm max} = 0.1\,h^{-1}$ Mpc, respectively. The survey volume and mean number density of galaxies for each survey can be found in appendix E in Saga et al. (2022).

In this way, we obtain the marginalized constraint on the bias parameters, $\sigma_b = \sqrt{\left(F^{-1}\right)_{11}}$, which is used for a Gaussian prior to further constrain the LPI violation parameter α in equation (4).

This paper has been typeset from a TEX/LATEX file prepared by the author.